An IFNγ/STAT1/JMJD3 Axis Induces ZEB1 Expression and Promotes Aggressiveness in Lung Adenocarcinoma

Jianjian Yang, Xue Wang, Bing Huang, Rong Liu, Hui Xiong, Fan Ye, Chenxi Zeng, Xiangning Fu, and Lequn Li

ABSTRACT

Active IFNγ signaling is a common feature of tumors responding to PD-1 checkpoint blockade. IFNγ exhibits both anti- and protumor activities. Here, we show that the treatment of lung adenocarcinoma cells with IFNγ led to a rapid increase of ZEB1 expression and a significant change in epithelial-to-mesenchymal transition (EMT)-associated gene expression pattern. Moreover, functional analyses show that IFNγ promoted cell migration *in vitro* and metastasis *in vivo*. We demonstrate that ZEB1 is required for IFNγ-promoted EMT, cell migration, and metastasis, as RNAi-mediated knockdown of ZEB1 abrogated EMT, cell migration, and metastasis induced by IFNγ. We show that IFNγ induced upregulation of JMJD3 significantly reduced H3K27 trimethylation in the promoter of the *ZEB1* gene, which led to activation of *ZEB1* gene transcription. IFNγ-induced JMJD3 expression was JAK1/2-STAT1 dependent. Inhibition of JMJD3 abrogated IFNγ-induced ZEB1 expression. IFNγ-induced ZEB1 also reduced *miR-200* expression. Downregulation of ZEB1 increased *miR-200* expression, which led to a reduction of PD-L1 expression induced by IFNγ. It is worth noting that knockdown of *ZEB1* did not affect IFNγ-mediated antiproliferation and induction of CXCL9 and CXCL10. Thus, downregulation of ZEB1 may prevent the protumor activity of IFNγ while retaining its antitumor function. This study expands our understanding of IFNγ-mediated signaling and helps to identify therapeutic targets to improve current immunotherapies.

Implications: IFNγ increases ZEB1 expression in a STAT1-JMJD3 dependent manner, and consequently promotes cancer cell aggressiveness. This study provides a potential target to minimize the procancer effect of IFNγ while preserving its antitumor function.

Introduction

The inhibition of PD1/PD-L1 has led to a paradigm shift in the treatment of lung adenocarcinoma. Important consequences of PD1/PD-L1 blockade are increased T-cell function and IFNγ production (1). IFNγ is one of the essential cytokines in antitumor immunity and immunotherapies. IFNγ has direct tumor cell-specific antitumor effects, such as cell-cycle arrest and the subsequent inhibition of lung cancer cell proliferation (2). Garris and colleagues have demonstrated that effective anti-PD-1 cancer immunotherapy requires T-cell–dendritic cell crosstalk and involves the cytokines IFNγ and IL12 (3). Genomic defects in the IFNγ pathway in tumor cells, including mutations in both IFNγ receptors, JAK2, and the IFNγ signaling downstream protein IRF1, contribute to resistance to immunotherapy (4–6). IFNγ promotes CXCL9, CXCL10, and CXCL11 expression, thereby increasing the recruitment of CXCR3^{+} T cells into the tumor microenvironment, which plays a crucial role in determining the effectiveness of immunotherapy (7, 8).

Despite the pivotal role of IFNγ in antitumor host immunity, under certain circumstances, IFNγ induces tumor progression (9). IFNγ, like most cytokines, induces inhibitory feedback mechanisms to restrain the magnitude of the immune response (1). For instance, the high concentration of IFNγ produced by functional cytolytic T cells induces PD-L1 expression, which enables tumor cells to acquire the capability to counterattack immune cells (10, 11). Sustained IFN signaling in tumor cells triggers STAT1-dependent epigenetic and transcriptional changes, which consequently lead to the expression of multiple ligands for T-cell inhibitory receptors besides PD-1/PD-L1, which in turn confers tumor resistance to PD-1/PD-L1-based immunotherapy (12). Moreover, very recently, IFNγ has been reported to induce epithelial-to-mesenchymal transition (EMT) in prostate cancer and renal cancer and stimulate metastasis. In these cases, IFNγ regulates the turnover of specific tumor-suppressive microRNAs, such as miR-363 in particular, through the upregulation of the IFN-stimulated gene IFN-induced tetratricopeptide repeat 5 (*IFIT5*), consequently leads to EMT in cancer cells (13).

EMT has long been associated with the acquisition of malignant cell traits, such as motility and invasiveness (14). EMT is executed by EMT activating transcription factors (EMT-TF), mainly of the SNAIL, TWIST, and ZEB families (15). These transcription factors are also involved in cancer initiation, cancer cell plasticity, and cancer progression (16, 17). It remains unclear whether IFNγ induces EMT-TF expression and promotes EMT in lung adenocarcinoma cells. In this study, we showed that IFNγ upregulated ZEB1 expression and promoted EMT in lung cancer cells. We found that IFNγ stimulation resulted in induction of JMJD3, decreased H3K27 trimethylation in the promoter region of the *ZEB1* gene, and consequently increased ZEB1 expression. Knockdown of *ZEB1* in lung adenocarcinoma cells eliminated IFNγ-mediated protumor effects while retaining its antitumor functions.

Thoracic Surgery Laboratory, Department of Thoracic Surgery, Tongji Hospital, Tongji Medical College, Huazhong University of Science and Technology, Hubei, China.

Corresponding Authors: Lequn Li, Department of Thoracic Surgery, Huazhong University of Science and Technology, Wuhan, 430030, China. E-mail: lqli@tjh.tjmu.edu.cn; and Xiangning Fu, fuxn2006@aliyun.com

Materials and Methods

Cell lines and cell culture

Human lung adenocarcinoma A549 (ATCC Catalog No. CRL-7909, RRID: CVCL_0023), HCC827 (KCLB Catalog No. 70827, RRID: CVCL_2063), H1975 (ATCC Catalog No. CRL-5908, RRID: CVCL_1511), H2228 (ATCC Catalog No. CRL-5935, RRID: CVCL_1543), H1573 (ATCC Catalog No. CRL-5877, RRID: CVCL_1478), H2444 (ATCC Catalog No. CRL-5945, RRID: CVCL_1552), and UMC-11(ATCC Catalog No. CRL-5975, RRID: CVCL_1784) cell lines were obtained from Cobioer Biosciences. Short tandem repeat (STR) analysis was performed for A549, HCC827, and H1975 cell lines in 2017 and other cell lines in 2019 (Cobioer Biosciences). All of the cell lines were confirmed to be mycoplasma negative (Biothrive Sci. & Tech. Ltd.). Lung adenocarcinoma cells were maintained as a monolayer culture in RPMI1640 (GIBCO) supplemented with 10% FBS (GIBCO) and 1% penicillin/streptomycin (Hyclone).

Patients and tissue samples

Lung adenocarcinoma specimens were obtained from 42 patients, who underwent pulmonary resection prior to radiation or chemotherapy in the Department of Thoracic Surgery, Tong Ji Hospital. Histologic diagnosis of tumors was based on the WHO criteria. The TNM stage was determined according to the 7th Edition AJCC staging guidelines. This research was performed in accordance with the Helsinki Declaration. The use of human tissue samples was approved by the Institutional Ethics Committee of the Huazhong University of Science and Technology. Each patient signed written informed consent on the day of admission.

Antibodies and reagents

All of the antibodies and reagents are listed in Supplementary Table S1.

RNA isolation and qRT-PCR analysis

The TRizol method was used to isolate total RNA. TRizol was obtained from TAKARA. RNA was reverse transcribed into cDNA using the RT Reagent Kit according to the manufacturer's protocol (Vazyme Biotech Co.). qRT-PCR was carried out using Fast SYBR Green Master Mix (Life Technologies). The primers were obtained from TsingKe Biological Technology. The primer sequences are presented in Supplementary Table S2. Negative controls without template were included, and all of the reactions were conducted in triplicate. β-Actin was used as internal control. Relative expression of target genes was determined by the $2^{-\Delta\Delta Ct}$ method.

siRNA transfection

siRNA sequences specifically targeting JAK1, JAK2, STAT1, ZEB1, and JMJD3 were synthesized by RiboBio. siRNA (50 nmol/L) and Lipofectamine 3000 (Life Technologies) were gently premixed in medium without FBS as per the guidelines. Knockdown efficacy was evaluated using RT-PCR and immunoblotting.

Preparation of short hairpin RNA (shRNA) and cell transfection

The shRNA sequence targeting ZEB1 (shRNA-ZEB1) was 5′-GAACCAGTTGTAAATGTAA-3′. shRNA-ZEB1 was inserted in the GV493 vector (hU6-MCS-CBh-gcGFP-IRES-puromycin; GeneChem). Empty GV493 vector was used as a negative control. Knockdown of ZEB1 was confirmed by RT-PCR and immunoblotting.

RNA-seq

Total RNA was isolated from cells using the RNeasy Mini Kit (Qiagen). Paired-end libraries were synthesized using the VAHTS stranded mRNA-seq Library Prep Kit for Illumina (Vazyme) following the manufacturer's guidelines. Briefly, the poly-A containing mRNA molecules were purified using poly-T oligo-attached magnetic beads. Purified libraries were quantified with a Qubit 2.0 Fluorometer (Life Technologies) and validated with an Agilent 2100 bioanalyzer (Agilent Technologies) to confirm the insert size and calculate the mole concentration. Clusters were generated by cBot with the library diluted to 10 pmol/L and sequenced on Illumina HiSeq X-ten (Illumina). Library construction and sequencing were performed at Shanghai Biotechnology Corporation. The RNA-seq data have been deposited in the Gene Expression Omnibus database [Gene Expression Omnibus (GEO), RRID: SCR_005012] under accession code GSE150255.

Western blotting

Cells were lysed and proteins were separated by SDS-PAGE and transferred to Immobilon-P membranes (Millipore). The blots were developed using the ECL detection system (Advansta). To ensure that equal amounts of sample protein were applied per lane, β-actin was used as loading control.

Histone extraction

Cells were harvested and washed twice with ice-cold PBS. Subsequently, cells were resuspended in Triton Extraction Buffer (TEB: PBS containing 0.5% Triton X-100 and 2 mmol/L PMSF) at a cell density of 10^7 cells/mL. Then the cells were lysed on ice for 10 minutes with gentle stirring, and centrifuged at $400 \times g$ for 10 minutes at 4°C. The cell pellet was resuspended in 0.2N HCl at a cell density of 4×10^7 cells/mL at 4°C overnight. The samples were centrifuged at $400 \times g$ for 10 minutes at 4°C, and the supernatant was used for immunoblot analysis.

Immunofluorescence staining of cultured cells

Cells cultured on cover slides were pretreated with indicated reagents for 72 hours. The cells were fixed with 4% paraformaldehyde for 20 minutes, permeabilized with 0.1% Triton X-100 for 10 minutes, blocked with 5% BSA for 0.5 hours, and labeled with primary antibody at 4°C overnight. The cells were staining with secondary antibody for 0.5 hours at room temperature, and cells were counterstained with DAPI for 10 minutes at room temperature. Cells were visualized with a fluorescence microscope (Olympus).

Cell proliferation assay

Cell proliferation was assessed using the CCK-8 Kit (Dojindo Molecular Laboratories). Cells were seeded (3,000–5,000 in 100 μL/well) and cultured overnight before exposure to the indicated stimuli. Absorbance was measured at 450 nm using a microplate spectrophotometer (TECAN).

Colony-formation assay

Cells were seeded in 6-well plates at a density of 800 cells/well and maintained for 14 days with or without IFNγ (100 IU/mL). The cells were fixed with 4% (w/v) paraformaldehyde for 20 minutes, stained with crystal violet for 15 minutes, and washed with PBS three times.

Transwell migration assay

The cell migration assay was carried out using 8 μm pore size Transwell chambers (Corning). In brief, cells were suspended in

serum-free medium and plated into the upper chambers (7×10^4 cells in 100 μL/well). In the lower chambers, medium supplemented with 10% FBS was used as a chemo-attractant. IFNγ and other indicated reagents were added to both chambers at equal concentrations. After 24 hours of incubation, the cells that migrated through the membrane to the bottom surface were fixed with 4% (w/v) paraformaldehyde, and stained with 0.1% (w/v) crystal violet. The migratory cells were examined under an optical microscope at 200× magnification. The average numbers of migratory cells were obtained from three randomly chosen fields.

ELISA

ELISA was performed using a CXCL-10 ELISA kit (Ruixin Biotech) according to the manufacturer's instructions.

Chromatin immunoprecipitation (ChIP)

The ChIP assay was performed using ChIP Kit, following the manufacturer's instructions (Cell Signaling Technology). Immunoprecipitation was performed overnight at 4°C with anti-H3K27me3 (Active Motif Catalog No. 39155, RRID: AB_2561020) and anti-H3K4me3 (Active Motif Catalog No. 39915, RRID: AB_2687512) antibodies, and a normal rabbit IgG (Cell Signaling Technology; Catalog No. 2729, RRID: AB_1031062) control. The fragments of the human *ZEB1* promoter in immunoprecipitates were identified by qPCR. Detailed information on primers is provided in Supplementary Table S2.

Animal model

All of the animal experiments were approved by the Animal Care Committee of Tongji Hospital (approval number: TJH-201902001). NCG mice were purchased from the Experimental Animal Center (Hubei, China) and maintained in an environment with a standardized barrier system (System Barrier Environment No. 00021082). A549 cells, A549-shRNA-control cells, and A549-shRNA-ZEB1 cells pretreated with IFNγ (400 IU/mL) for 4 days or without IFNγ treatment were resuspended in 100 μL PBS and then injected into the tail vein of NCG mice (2×10^6 cells/mouse), followed by intraperitoneal injection of IFNγ (2,000 IU in 100 μL per mouse) every other day for total three times. Histologically detectable lung metastatic foci were observed microscopically 7 days postinjection (18). The lungs were excised, fixed in 10% formalin, paraffin-embedded, and stained with hematoxylin and eosin (H&E) for pathologic identification of tumor nodules in the lung parenchyma. The photomicrographs of the lungs were taken using a light microscope (Axio Observer 3; Zeiss). The metastasis area and lung area were quantified using ImageJ (ImageJ, RRID: SCR_003070) software.

Ex vivo culture of patient-derived lung cancer explants

Fresh lung cancer tissues were obtained from patients undergoing pulmonary resection prior to radiation or chemotherapy in the Department of Thoracic Surgery, Tongji Hospital. The *ex vivo* culture was performed as described previously (19). Briefly, fresh human lung cancer tissue was dissected into 1 mm³ cubes, placed on a Gelatin sponge (HuSHiDa), and bathed in RPMI1640 medium supplemented with 10% heat-inactivated FBS and 100 IU/mL penicillin–streptomycin. In addition, indicated amounts of IFNγ were added to the media. Tissues were cultured at 37°C for 24 to 36 hours and collected for RNA extraction.

Statistical analysis

Data in bar graphs are displayed as mean ± SD. Data between two groups were compared with the two-tailed Student *t* test (*$P < 0.05$, **$P < 0.01$, ***$P < 0.001$), and one-way ANOVA was used to compare data between three or more groups. The association between *ZEB1* and *IFNG* mRNA levels was assessed by Pearson correlation test. Statistical analysis was performed with GraphPad Prism software v. 8.0 (Graph-Pad Prism, RRID: SCR_002798). For RNA-seq data, the *P* value significance threshold in multiple tests was set by the FDR. Fold-changes were also estimated according to the FPKM value in each sample. The differentially expressed genes were selected using the following criteria: FDR ≤0.05 and $\log_2$ (fold-change) ≥0.5.

Results

IFNγ induces ZEB1 expression in lung adenocarcinoma

Previously, we performed a global transcriptome study (microarray analysis) and compared tumor tissues with high versus low *IFNG* expression levels. *ZEB1* mRNA levels were significantly higher in tumors with high *IFNG* expression (GSE99995). We examined the correlation between *IFNG* and *ZEB1* in a uniform cohort of a total of 42 patients with locally advanced lung adenocarcinoma (stage IIIA) from our patient archive (Supplementary Table S3). *IFNG* expression in tumors was significantly correlated with *ZEB1* expression (**Fig. 1A**; $n = 42$, $r = 0.3653$; $P = 0.0174$). Among these patients, 18 paraffin-embedded tumors were available for ZEB1 IHC analysis. The median *IFNG* expression was used to split patients into two groups (IFNG^hi, $n = 8$ vs. IFNG^low, $n = 10$). ZEB1 immunoreactivity was observed in both tumor stroma and tumor nests. Positive ZEB1 immunoreactivity in tumor nests was found in four samples. Three of them were from the IFNG^hi group (three of total eight tumors, 37.5%) and only one was from the IFNG^low group (1 of 10 tumors, 10%; Supplementary Fig. S1A). Next, to determine whether IFNγ could directly induce ZEB1 expression in lung cancer cells, A549 cells were treated with IFNγ. As shown in Supplementary Fig. S1B, ZEB1 protein expression was increased in A549 cells in response to IFNγ stimulation. IFNγ also upregulated *ZEB1* gene transcription in lung adenocarcinoma cells (**Fig. 1B**). IFNγ did not induce *ZEB1* expression in UMC-11 cells, a lung carcinoid cell line. Immunoblotting analysis revealed that ZEB1 protein levels increased within 12 hours upon IFNγ stimulation and sustained for at least 72 hours after a single treatment (**Fig. 1C**). Strikingly, prolonged exposure of A549 and H1975 to IFNγ led to sustained ZEB1 expression even after removal of IFNγ (**Fig. 1D**).

Finally, we cultured human-derived lung adenocarcinoma *ex vivo* to confirm the effect of IFNγ on ZEB1 expression. IFNγ induced the transcription of the *ZEB1* gene in tumors but not in distant nontumor lung tissues (**Fig. 1E**). Our data demonstrate that IFNγ upregulates ZEB1 expression at both mRNA and protein levels in lung adenocarcinoma cells.

IFNγ induces EMT in lung adenocarcinoma cells

E-cadherin and Vimentin are the most commonly used EMT markers, as their expression patterns undergo dramatic changes during EMT. IFNγ stimulation downregulated E-cadherin expression and upregulated Vimentin expression, as determined by immunoblot analysis (**Fig. 2A**). The altered expression patterns of E-cadherin and Vimentin in lung cancer cells upon IFNγ treatment were further validated by immunofluorescence analysis (**Fig. 2B**). RT-PCR analysis
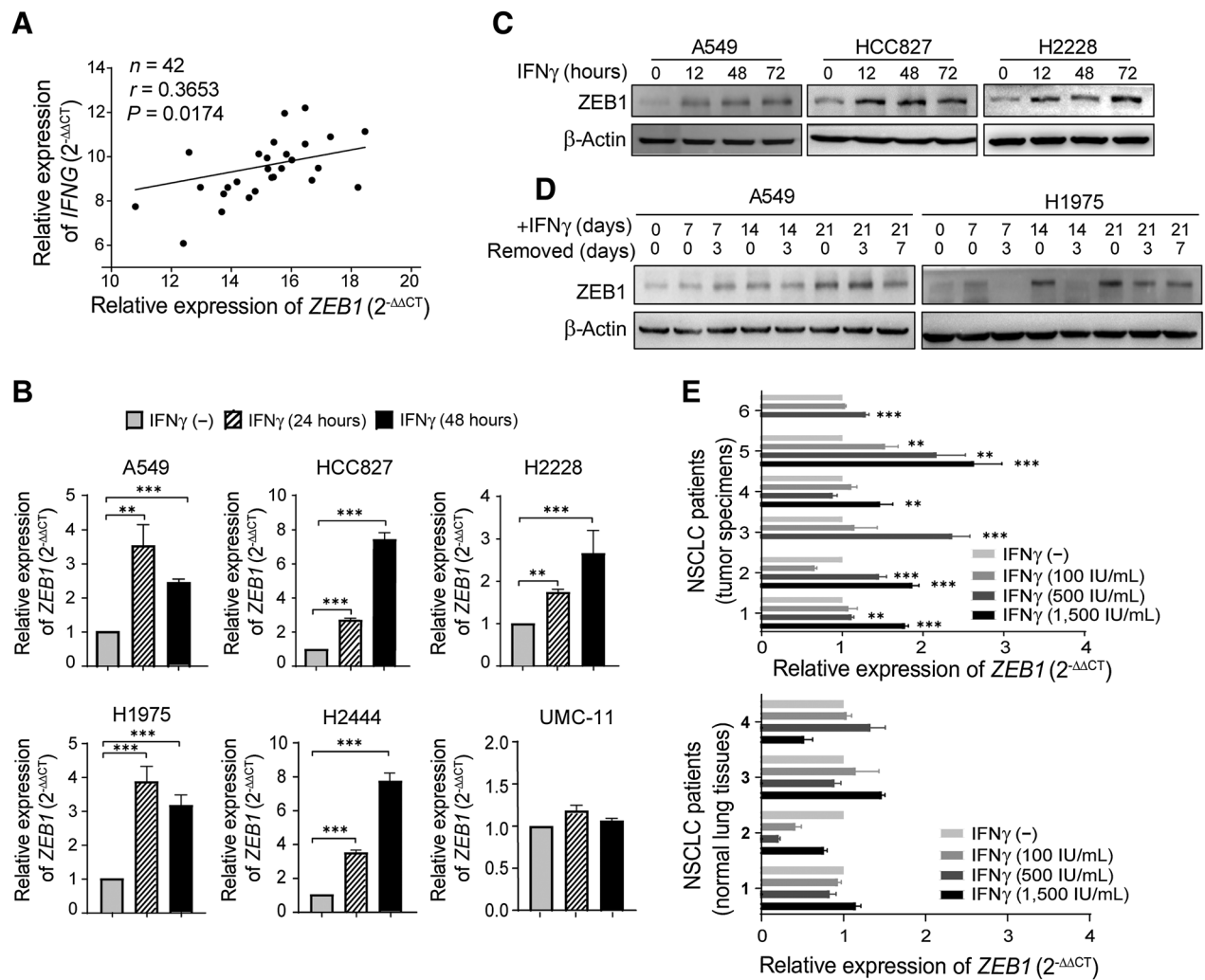
Figure 1.
IFNγ upregulates ZEB1 expression in lung adenocarcinoma cells. **A,** *ZEB1* and *IFNG* mRNA expression in tumor tissues from 42 patients with lung adenocarcinoma was evaluated by qRT-PCR. **B,** *ZEB1* mRNA expression was quantified by qRT-PCR. **C,** ZEB1 protein expression was analyzed by immunoblotting. Data shown are representative images of four independent experiments. **D,** Cells were cultured with IFNγ (25 IU/mL) for indicated time intervals. IFNγ was removed for 3 or 7 days. ZEB1 expression was analyzed by immunoblotting. **E,** Fresh human lung cancer tissue ($n = 6$) and distant nontumor lung tissues (>3 cm away from the edge of the tumors; $n = 4$) were treated with indicated concentrations of IFNγ for 36 hours, and the tissues were collected for RNA extraction. *ZEB1* mRNA expression was quantified by qRT-PCR. Data are presented as mean ± SD ($n = 3$) and were analyzed by the two-sided Student t test (*, $P < 0.05$; **, $P < 0.01$; ***, $P < 0.001$).

revealed that *CDH1* transcription was decreased at 24 hours and maintained at a low level in A549 and H2228 cells, whereas *VIM* transcription was significantly increased to various degrees in the three cell lines in response to IFNγ stimulation (**Fig. 2C**).

Treatment with low amounts of IFNγ (10 IU/ml) for 3 days did not significantly affect E-cadherin levels in A549 and HCC827 (Supplementary Fig. S1C). Although treatment with IFNγ at 25 IU/ml significantly downregulated E-cadherin levels in A549 and HCC827 cells (Supplementary Fig. S1D). Prolonged exposure to IFNγ induced morphologic changes in A549 and HCC827 cells, which acquired a fibroblast-like appearance (**Fig. 2D**), indicating that IFNγ-treated cells enter a stable mesenchymal-associated state. Substantial evidence has shown that EMT is associated with increased cell migration *in vitro*. As shown in **Fig. 2E**, the migratory capability of A549 and HCC827 cells was indeed significantly increased after IFNγ treatment. Collectively,

these data demonstrate that IFNγ induces EMT in lung adenocarcinoma cells and promotes cell migration *in vitro*.

IFNγ-induced ZEB1 expression stimulates EMT

EMT involves a robust reprogramming of gene expression. We analyzed the transcriptome alterations by RNA-seq analysis during EMT following IFNγ treatment. It has been reported that A549 cells have mesenchymal characteristics, whereas HCC827 cells have epithelial features (20). For these reasons, we selected A549 and HCC827 cells to investigate the reprogramming of gene transcription by IFNγ. An EMT signature consisting of 130 genes was analyzed, including 67 upregulated mesenchymal-associated genes and 63 downregulated epithelial-associated genes (Supplementary Table S4; ref. 21). Of the 63 epithelial-associated genes, 35 genes including *CDH1*, were highly expressed in HCC827 cells compared with A549 cells; of the 67
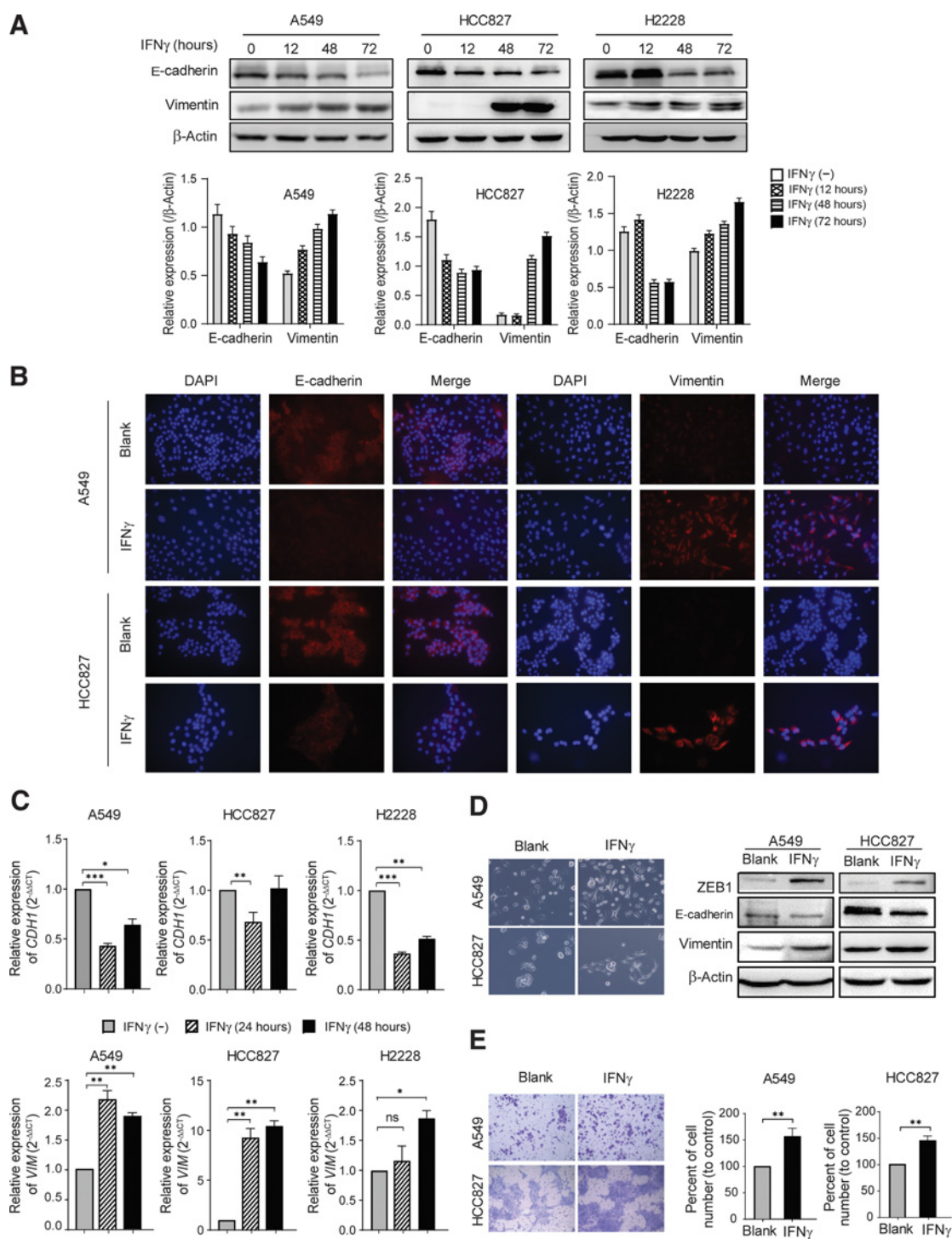
Figure 2.
IFNγ induces EMT in lung adenocarcinoma cells. **A,** The protein levels of E-cadherin and Vimentin in cells treated with IFNγ were analyzed by immunoblotting. The bar graphs show densitometry analyses of changes in E-cadherin and Vimentin levels as normalized to β-actin. Data shown are representative images of four independent experiments. **B,** Cells were treated with or without IFNγ (100 IU/mL) for 72 hours, and immunostained with anti-E-cadherin (1:200) or anti-Vimentin (1:200). Blank indicates untreated cells (magnification, 200×). **C,** Cells were treated with or without IFNγ (100 IU/mL) for 24 and 48 hours. *CDH1* and *VIM* mRNA levels were quantified by qRT-PCR. Data are presented as mean ± SD (*n* = 3) and were analyzed by the two-sided Student *t* test (*, *P* < 0.05; **, *P* < 0.01; ***, *P* < 0.001; ns, not significant). **D,** A549 and HCC827 cells were treated with or without IFNγ (25 IU/mL) for 2 weeks. Changes in cell morphology were observed by phase-contrast light microscopy (magnification, 200×). **E,** The effect of IFNγ on cell migration was examined by Transwell assay. Cells (7 × 10⁴ in 100 µL serum-free medium) were treated with or without IFNγ (100 IU/mL) for 24 hours. The number of cells on the bottom side of the Transwell inserts was counted in three random fields under a light microscope (magnification, 200×).

Figure 3.
IFNγ-induced ZEB1 expression is responsible for EMT. Changes in the expression of EMT-associated genes in A549 and HCC827 cells are shown. **A,** Comparison of expression profiles of EMT-associated genes between A549 and HCC827. Red dots represent EMT-associated genes upregulated in HCC827 cells and blue dots indicate downregulated genes in HCC827 cells compared with A549 cells. Changes in the expression of EMT-associated genes in (**B**) A549 and (**C**) HCC827 cells in response to IFNγ stimulation (100 IU/mL) are shown. Red dots indicate upregulated genes and blue dots represent downregulated genes in response to IFNγ stimulation for 24 hours, compared with untreated cells. **D,** A549 and HCC827 cells were treated with IFNγ (100 IU/mL) for 24 hours. The mRNA levels of *CTGF, FGF2, MAP1B,* and *ABLIM1* were quantified by qRT-PCR. **E,** A549 and HCC827 cells were transfected with siRNA-ZEB1 or siRNA-control for 24 hours. The mRNA levels of *VIM* were quantified by RT-PCR. Data are presented as mean ± SD ($n = 3$) and were analyzed with one-way ANOVA; ***, $P < 0.001$). **F,** siRNA-ZEB1 or siRNA-control transfected A549 and HCC827 cells were stimulated with or without IFNγ (100 IU/mL) for 48 hours. Expression levels of ZEB1, E-cadherin, and Vimentin were analyzed by immunoblot.

mesenchymal-associated genes, 35 genes, including *VIM*, were expressed at lower levels in HCC827 cells than in A549 cells (**Fig. 3A**). These results indicate that relative to A549 cells, HCC827 cells have more epithelial-associated features, which was consistent with the reports by others (20). EMT is a dynamic process with intermediary states that are not easily identified in cultured cells. We performed transcriptome analysis after the cells were treated with IFNγ for 8 or 24 hours. The number of differentially expressed genes was dramatically increased after 24 hours of stimulation with IFNγ compared with 8 hours of stimulation (Supplementary Fig. S2).

In A549 cells, 58 genes were differentially expressed after 24 hours of IFNγ treatment, including 20 upregulated and 38 downregulated genes [Log$_2$(FC) ≥ 0.5, $P < 0.05$; **Fig. 3B**; Supplementary Table S5]. Among these differentially expressed genes, of 67 genes that are upregulated in EMT, 13 genes were upregulated after IFNγ treatment, and of 63 genes that are downregulated in EMT, 23 genes were downregulated after IFNγ treatment. In HCC827 cells, 58 genes were differentially expressed after 24 hours of IFNγ treatment, including 32 upregulated and 26 downregulated genes [Log$_2$(FC) ≥ 0.5, $P < 0.05$; **Fig. 3C**; Supplementary Table S6]; among these differentially expressed genes, of 67 genes that upregulated in EMT, 21 genes were upregulated after IFNγ treatment, and of 63 genes that are downregulated in EMT, 12 genes were downregulated after IFNγ treatment. Detailed analysis revealed that IFNγ stimulation of the mesenchymal-like A549 cells led to downregulation of more epithelial-associated genes (genes downregulated during EMT), whereas IFNγ stimulation of the epithelial-like HCC827 cells led to upregulation of more mesenchymal-associated genes (genes upregulated during EMT). Although IFNγ altered the expression patterns of E-cadherin and Vimentin in both A549 and HCC827 cells, transcriptome analysis of EMT-associated genes in IFNγ-treated cells revealed that IFNγ induced EMT in lung cancer cells is not a unified state. The characteristics of IFNγ-induced EMT could be associated with the intrinsic state of untreated lung cancer cells.

Although IFNγ differentially alters the expression of EMT-associated genes in A549 and HCC827 cells, RNA-seq analysis showed that the expression of 15 genes was equally affected in both cell lines upon IFNγ treatment, including 7 upregulated and 8 downregulated genes. Among the upregulated genes, *CTGF*, which encodes connective tissue growth factor (CTGF), can induce EMT and its expression levels are highly correlated with EMT markers (22). *FGF2*, which encodes basic fibroblast growth factor, and *MAP1B*, which encodes a protein belonging to the microtubule-associated protein family, are both upregulated during EMT (21). FGF2 promotes EMT and metastasis through the FGFR1–ERK1/2–SOX2 axis in FGFR1-amplified

lung cancer (23). Actin binding LIM protein 1, encoded by the *ABL1M1* gene, plays multiple roles in establishing and maintaining cellular structure through mediating interactions between actin filaments and cytoplasmic LIM binding partners (24). *ABLIM1* is downregulated during EMT (21). These differentially expressed genes in response to IFNγ stimulation in both A549 and HCC827 cells were confirmed by qRT-PCR (**Fig. 3D**).

To determine whether ZEB1 is involved in IFNγ induced EMT, we knocked down *ZEB1* using siRNA and we found that knockdown of *ZEB1* abrogated the IFNγ-induced upregulation of *VIM* transcription (Supplementary Figs. S3A and S3E). IFNγ-mediated alterations in the expression pattern of E-cadherin and Vimentin in A549 and HCC827 cells were reversed upon *ZEB1* knockdown (**Fig. 3F**).

ZEB1 is required for IFNγ-promoted cell migration and metastasis

The migratory capability of A549 cells promoted by IFNγ was significantly compromised by the downregulation of ZEB1 expression (**Fig. 4A**). To examine the *in vivo* effects of IFNγ on lung cancer cell metastasis, we established an *in vivo* metastasis model by intravenous injection of A549 cells that had been treated with IFNγ *in vitro* for 4 days into NCG mice (2×10^6 cells/mouse) (**Fig. 4B**). The mice were given recombinant human IFNγ (2,000 IU/mouse) intraperitoneally every other day for a total of three times. Seven days after injection of A549 cells, lung tissues were collected and the presence of metastatic foci and the size of metastases were analyzed microscopically. Control mice were given untreated A549 cells and the mice were not given IFNγ. As shown in **Fig. 4C**, IFNγ treatment significantly increased the number and the size of metastatic nodules in lung tissues.

To determine the role of ZEB1 in this event, we transfected A549 cells with shRNA against *ZEB1* (shRNA-ZEB1) and obtained a stable *ZEB1*-depleted cell line (Supplementary Fig. S3B). The IFNγ-promoted increase of A549 cell migration *in vitro* was diminished in shRNA-ZEB1 A549 cells (**Fig. 4D**). Our *in vivo* metastasis model showed that the number and the size of metastatic nodules were reduced in mice injected with IFNγ-treated shRNA-ZEB1 A549 cells compared with mice injected with IFNγ-treated control A549 cells, indicating that loss of *ZEB1* dramatically reduces IFNγ-promoted metastasis of A549 cells (**Fig. 4E**). Our data demonstrate that ZEB1 is responsible for IFNγ-induced cell migration *in vitro* and metastasis *in vivo*.

IFNγ-induced upregulation of JMJD3 enhances *ZEB1* transcription via demethylation of H3K27 in the promoter of the *ZEB1* gene

We next evaluated whether IFNγ-induced activation of the JAK1/2–STAT1 pathway is involved in the regulation of ZEB1 expression. We knocked down JAK1, JAK2, and STAT1 using siRNA in A549 and HCC827 cells, and these cells were subsequently stimulated with IFNγ. Upregulation of ZEB1 by IFNγ was no longer observed in the knockdown of *JAK1, JAK2,* and *STAT1* cells (**Fig. 5A–C**).

ZEB1 transcription is regulated by the modulation of the chromatin environment at gene regulatory elements (25, 26). H3K27me3 is often associated with transcriptional repression. The relative absence of H3K27me3 in the chromatin at the *ZEB1* promoter signals active transcription (25). Interestingly, the expression of H3K27 trimethylation and the ratio of H3K27me3 to H3 was rapidly reduced in A549 cells after exposure to IFNγ (**Fig. 5D**). JMJD3, a direct transcriptional target of STAT1, catalyzes the demethylation of H3K27me3 (27). For these reasons, we examined whether IFNγ induces JMJD3 expression. *JMJD3* transcription was rapidly upregulated in A549 and HCC827

cells upon exposure to IFNγ (**Fig. 5E**). Immunoblot analysis revealed increased JMJD3 expression after 3 hours of IFNγ treatment (**Fig. 5F**). To determine whether JMJD3 is associated with IFNγ-induced ZEB1 expression, the JMJD3-specific inhibitor GSK-J4 was used (28). To determine the proper amount of GSK-J4 to be used in our experimental setting, we evaluated the effect of GSK-J4 alone on H3K27me3 levels and ZEB1 expression. As shown in **Fig. 5G**, GSK-J4 at concentrations of 1 and 5 μmol/L significantly enhanced H3K27me3 levels but did not alter ZEB1 expression. However, GSK-J4 at 10 μmol/L did not increase H3K27me3 levels while enhancing ZEB1 expression significantly, suggesting that GSK-J4 at lower concentration serves as JMJD3 inhibitor and has no direct effect on ZEB1 expression. For these reasons, we used GSK-J4 at a concentration of 1 to 5 μmol/L to determine whether inhibition of JMJD3 activity prevents IFNγ-induced upregulation of ZEB1. As shown in **Fig. 5H**, additional GSK-J4 prevented IFNγ-induced upregulation of ZEB1 expression. Knockdown experiments with siRNA-JMJD3 further confirmed that IFNγ-induced ZEB1 expression requires JMJD3 (**Fig. 5I**). Downregulation of STAT1 expression led to abrogation of IFNγ-induced JMJD3 expression (**Fig. 5J**), confirming that IFNγ-induced JMJD3 expression is STAT1 dependent.

The *ZEB1* promoter exhibits a bivalent chromatin configuration (28). H3K4me3 is associated with transcriptional initiation (29), whereas H3K27me3 is associated with transcriptional repression. We performed a ChIP assay at the *ZEB1* promoter to compare the levels of histone modifications in control versus IFNγ-treated cells. IFNγ treatment led to a significant reduction in H3K27me3 levels at the *ZEB1* promoter in A549 cells, whereas IFNγ did not significantly affect H3K4me3 levels at the *ZEB1* promoter (**Fig. 5K**). These data demonstrate that IFNγ enables the *ZEB1* promoter to transition from the bivalent to the active chromatin state, at least in part through the demethylation of H3K27me3.

IFNγ-induced upregulation of ZEB1 leads to the downregulation of miR-200c

ZEB1 transcription is tightly regulated by miRNA. Recent studies have revealed that IFNγ promotes *ZEB1* expression through IFIT5-mediated suppression of miR-363 in prostate cancer and renal cancer (13). We did not observe the downregulation of *miR-363* expression by IFNγ in lung cancer cells (Supplementary Fig. S4). The *miR-200* family inhibits *ZEB1* expression and in turn, ZEB1 directly represses the transcription of *miR-200* loci (30). As shown in **Fig. 6A**, *miR-200c* expression was significantly reduced in A549 and HCC827 cells after 12 hours of IFNγ treatment, and the reduction of *miR-200c* expression was even more dramatic after 24 and 48 hours of IFNγ treatment. We wondered whether IFNγ-promoted *ZEB1* expression in lung cancer cells is related to the downregulation of *miR-200* expression. IFNγ-induced upregulation of *ZEB1* transcription was observed after 4 hours in both A549 and HCC827 cells, whereas *miR-200c* expression was not affected even after 6 hours of IFNγ stimulation (**Fig. 6B** and **C**). Moreover, increased ZEB1 protein expression was observed at 12 hours of IFNγ stimulation (**Fig. 1C**). Thus, our data suggest that IFNγ first promotes *ZEB1* transcription, and subsequently suppresses *miR-200c* expression.

Further analysis revealed that downregulation of *ZEB1* enhanced *miR-200* expression in IFNγ-treated cells compared with untreated cells (**Fig. 6E**). Knockdown of *ZEB1* also led to a significant reduction of IFNγ-induced PD-L1 expression in A549 and HCC827 cells (**Fig. 6D**). PD-L1 expression has been reported to be directly regulated by *miR-200* family members (31). Collectively, IFNγ stimulation rapidly induces ZEB1 expression and consequently downregulates

Figure 4.
IFNγ-promoted cell migration and metastasis are ZEB1-dependent. **A,** A549 cells were transfected with siRNA-ZEB1 or siRNA-control for 48 hours. Then the cells were treated with or without IFNγ and seeded in the upper chamber for the Transwell migration assay. After 24 hours, the cells in the lower chamber were counted in three random fields under a light microscope (magnification, 200×). Data are presented as mean ± SD and were analyzed with one-way ANOVA (**, $P < 0.01$). **B,** The establishment of an *in vivo* metastasis model by intravenous injection of A549 cells into NCG mice (2×10^6 cells/mouse). **C,** At the end of experimental period (7 days after intravenous injection of A549 cells), lung tissues were harvested and stained with hematoxylin and eosin (H&E). Representative images of histologic inspection of mouse lungs from each group are shown (magnification, 50×; insert, 200×). The number of tumor nodules and the lung metastasis index (ratio of tumor area to the total tumor and lung area) were evaluated and analyzed between IFNγ-treated and untreated groups. Data are presented as mean ± SD ($n = 3$) and were analyzed with the two-sided Student t test (*, $P < 0.05$). Scale bar: 200 μm. **D,** A549 cells were transfected with shRNA-ZEB1 or shRNA-control, and a stable *ZEB1* knockdown cell line was generated. Then the cells (7×10^4 cells in 100 μL RPMI1640) were suspended in serum-free medium with or without IFNγ (100 IU/mL) for 24 hours, the cells in the lower chamber were counted in three random fields under a light microscope (magnification, 200×). Data are presented as mean ± SD and were analyzed with one-way ANOVA (*, $P < 0.05$; **, $P < 0.01$; ns, not significant). **E,** A549 cells transfected with shRNA-ZEB1 or shRNA-control were injected into NCG mice via the tail vain, the animal model in **B** was used. Representative images of histologic inspection of mouse lungs from each group are shown (magnification, 50×; insert, 200×). The number of tumor nodules and lung metastasis index were calculated. The tumor nodules were counted and area ratio in the lung parenchyma was calculated. Data are presented as mean ± SD ($n = 3$) and were analyzed by one-way ANOVA (*, $P < 0.05$).
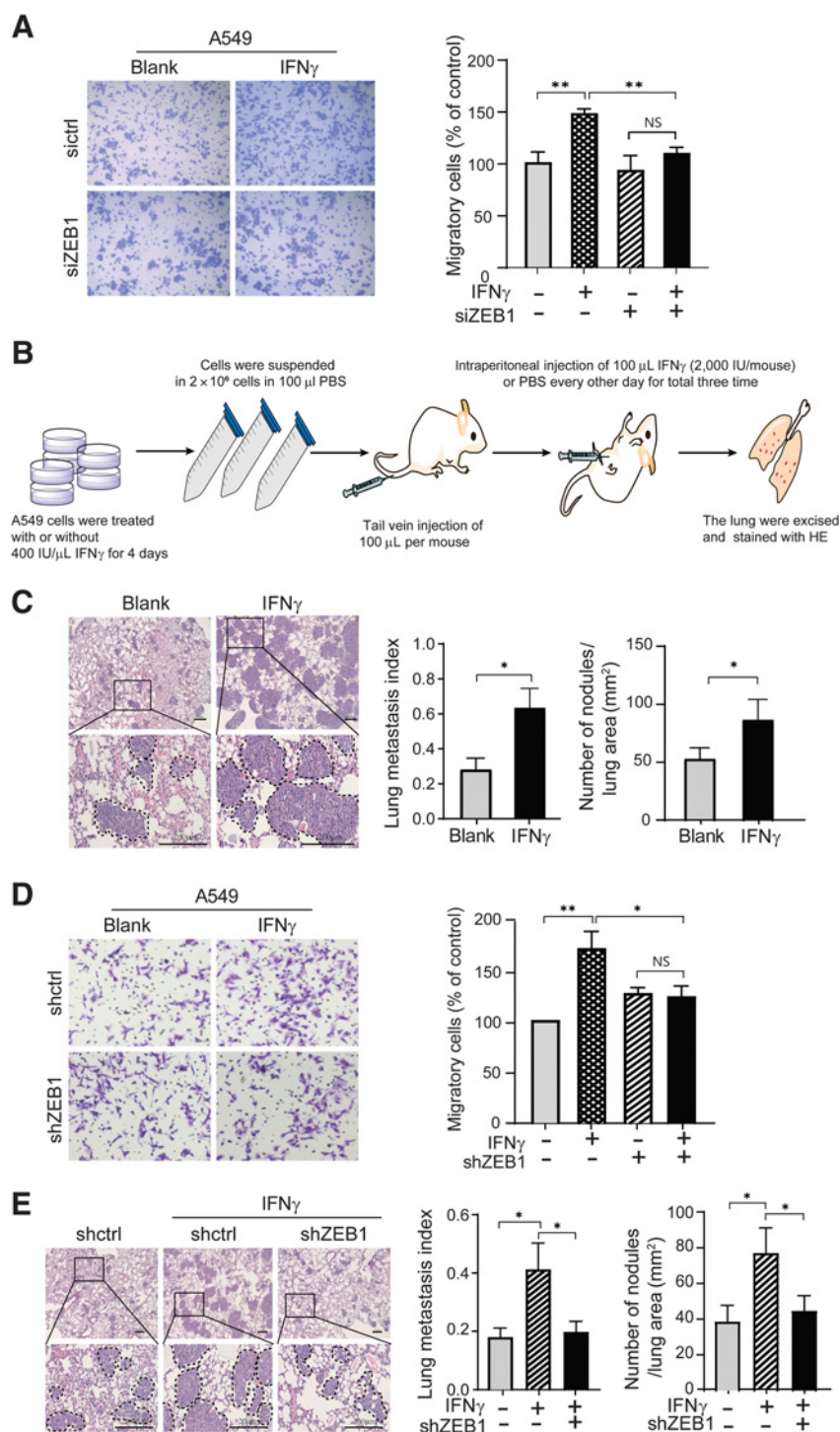

miR-200c, which at least partially contributes to the upregulation of PD-L1 expression.

IFNγ-mediated antiproliferative effects and induction of CXCL9 and CXCL10 expression are not affected by ZEB1 knockdown

Previous studies by us and others have shown that IFNγ suppresses the proliferation of lung cancer cells (2, 32). We wondered whether ZEB1 is involved in the IFNγ-mediated suppression of cell prolifer-

ation. Knockdown of *ZEB1* by siRNA did not alter the antiproliferative effects of IFNγ in both A549 and HCC827 cells (**Fig. 7A**). *ZEB1* knockdown did not affect IFNγ-mediated suppression of colony formation (**Fig. 7B**). Cyclin E1, which is encoded by the *CCNE1* gene, plays a critical role in the control of cell cycle progression by allowing G_1- to S-phase transition (33). IFNγ-treated A549 cells exhibited significantly lower *CCNE1* mRNA levels than untreated A549 cells. Knockdown of *ZEB1* did not affect IFNγ-mediated reduction of

Yang et al.
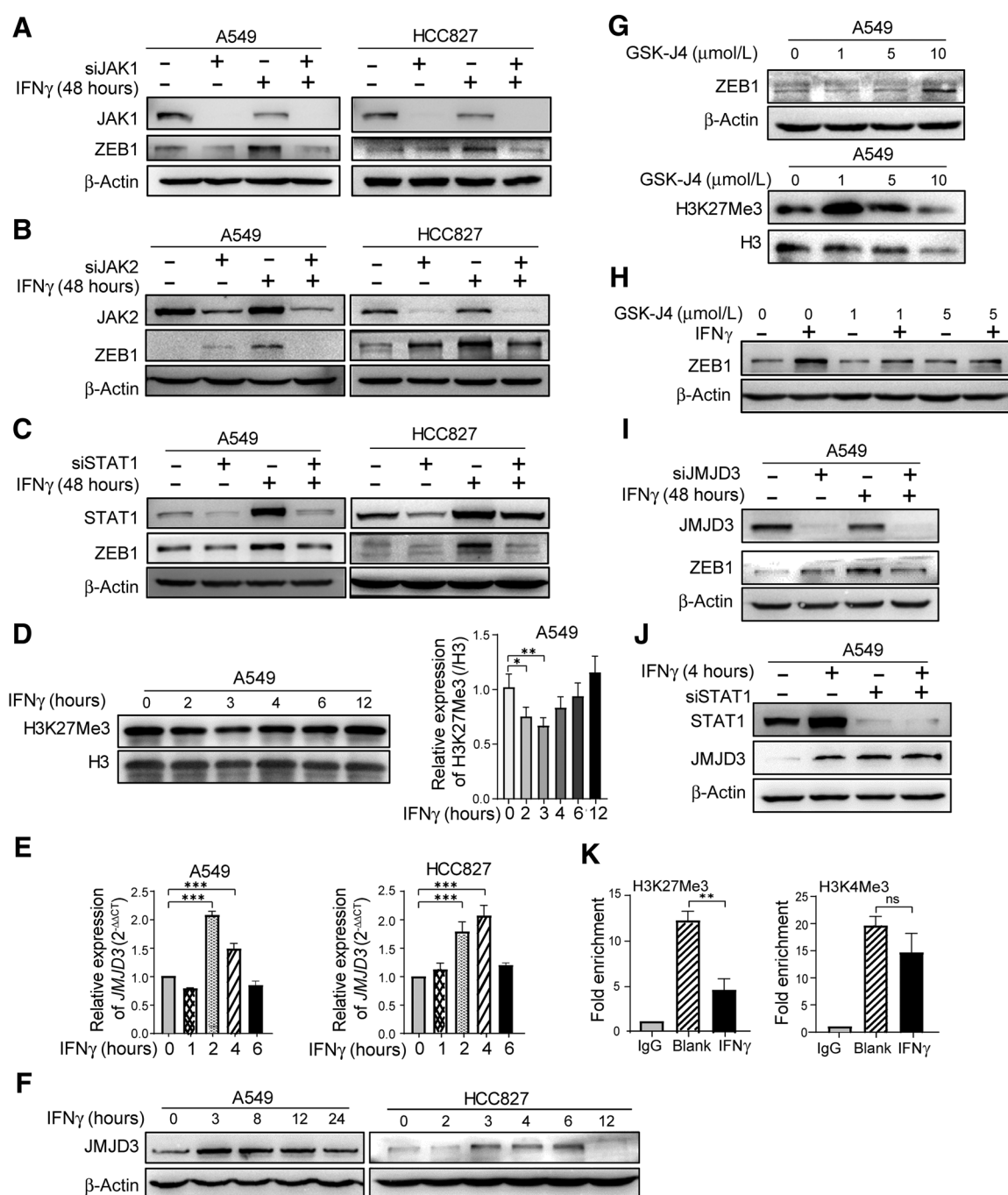
Figure 5.
IFNγ upregulates JMJD3 expression and enhances *ZEB1* gene transcription via demethylation of H3K27. A549 and HCC827 cells were transfected with (**A**) siRNA-JAK1, (**B**) siRNA-JAK2, or (**C**) siRNA-STAT1 and siRNA-control for 24 hours. Then the cells were cultured with or without IFNγ (100 IU/mL) for 48 hours. Subsequently, ZEB1 expression was analyzed by immunoblot. **D,** A549 cells were cultured with IFNγ for indicated time intervals and total histones were extracted following the Histone Extract protocol. H3K27me3 levels were analyzed by immunoblotting. The graph presents the quantification of H3K27me3 levels normalized to histone H3 levels. Data are presented as mean ± SD ($n = 3$) and were analyzed by one-way ANOVA (*, $P < 0.05$; **, $P < 0.01$). **E** and **F,** A549 and HCC827 cells were cultured with IFNγ (100 IU/mL). *JMJD3* mRNA levels were quantified by qRT-PCR. Untreated cells served as control (**E**). JMJD3 protein levels were analyzed by immunoblot (**F**). **G,** A549 cells were cultured with indicated concentrations of the JMJD3 inhibitor GSK-J4 for 24 hours, and ZEB1 and H3K27Me3 protein levels were analyzed by immunoblot. **H,** A549 cells cultured with or without GSK-J4 were treated with IFNγ. ZEB1 expression was analyzed by immunoblot. **I,** siRNA-JMJD3 or siRNA-control transfected A549 cells were treated with or without IFNγ (100 IU/mL) for 48 hours. ZEB1 expression was analyzed by immunoblot. **J,** siRNA-STAT1 or siRNA-control transfected A549 cells were treated with IFNγ (100 IU/mL) for 4 hours. JMJD3 expression was analyzed by immunoblot. **K,** A549 cells were treated with or without IFNγ for 4 hours, and harvested. ChIP-qPCR was performed for H3K4me3 and H3K27me3 histone modifications at the *ZEB1* promoter in A549 cells ($n = 3$). Data were analyzed with the two-sided Student *t* test (**, $P < 0.01$; ns, not significant).

Figure 6.

IFNγ regulates the *miR-200*/ZEB1 axis. A549 and HCC827 cells were cultured with IFNγ for indicated time intervals. The levels of *miR-200* in **A** and **B**, and *ZEB1* mRNA in **C** were quantified by RT-PCR. Data are presented as the mean ± SD ($n = 3$) and were analyzed with the two-sided Student *t* test (**, $P < 0.01$). **D** and **E,** Cells transfected with siRNA-*ZEB1* or siRNA-control were treated with or without IFNγ for 24 hours. ZEB1 and PDL1 expression was analyzed by immunoblot (**D**), and the levels of *miR-200c-3p* were quantified by RT-PCR (**E**; $n = 3$) and were analyzed with one-way ANOVA (**$P < 0.01$; ***$P < 0.001$).
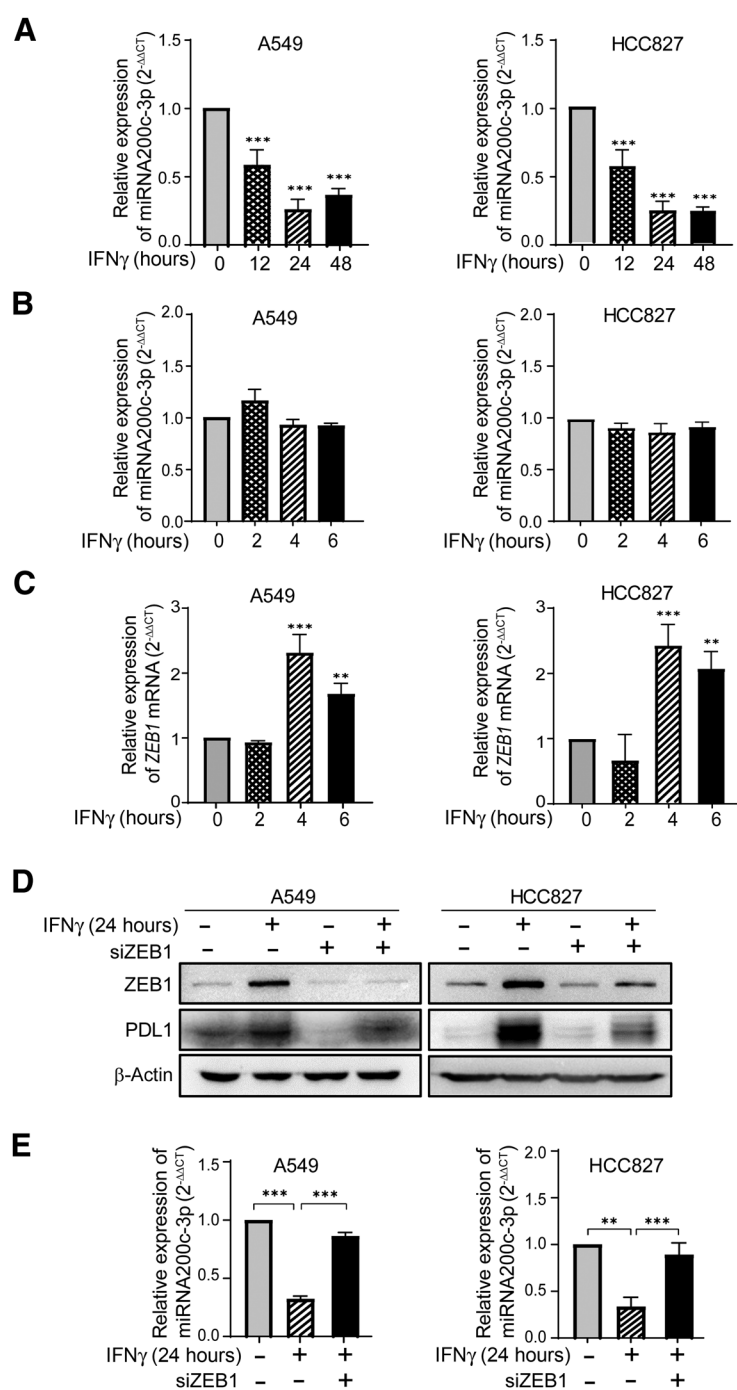
CCNE1 expression (**Fig. 7C**). IFNγ-mediated suppression of cell proliferation requires STAT1 and IRF1 (2). Downregulation of *ZEB1* had no effect on IFNγ-induced STAT1 and IRF1 expression at mRNA and protein levels (**Fig. 7D** and **E**). *ZEB1* knockdown did not affect IFNγ-induced phosphorylation of STAT1 (**Fig. 7F**). We also examined whether knockdown of ZEB1 affects STAT1-IRF1 target genes *CXCL9* and *CXCL10* expression. As shown in **Fig. 7G**, downregulation of ZEB1 expression did not alter the IFNγ-induced expression pattern of *CXCL9* and *CXCL10*. The results were con-firmed by ELISA analysis of CXCL10 expression at the protein level (**Fig. 7H**).

Discussion

The main findings of this study are summarized as follows: (i) IFNγ induces EMT in lung adenocarcinoma cells. RNA-seq analysis revealed that IFNγ stimulation altered the expression pattern of EMT-associated genes. Morphologic changes in lung adenocarcinoma cells

Yang et al.
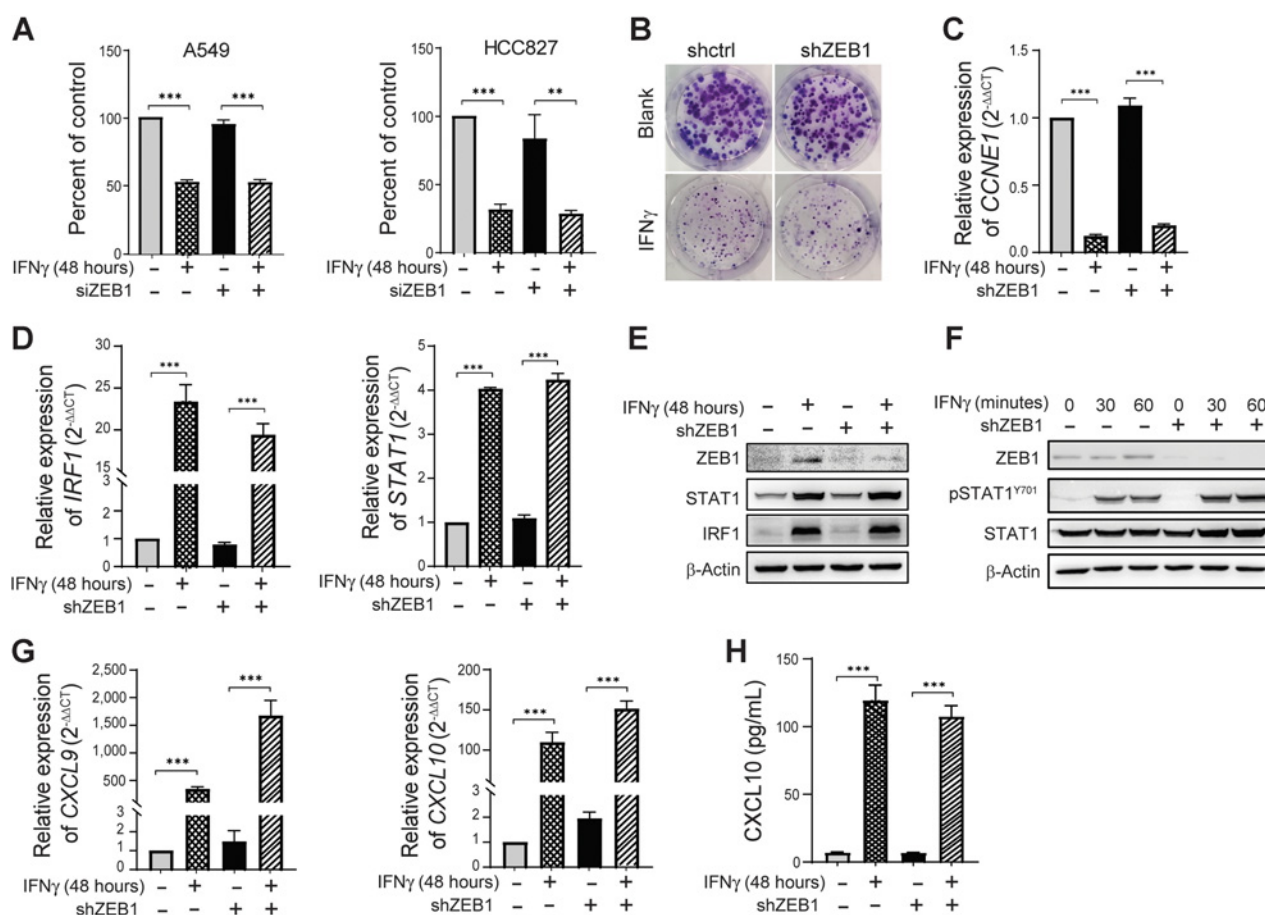
Figure 7.
Downregulation of ZEB1 expression does not affect the antitumor function of IFNγ. **A,** A549 and HCC827 cells were transfected with siRNA-control or siRNA-ZEB1 for 24 hours. Subsequently, the cells (5–10×10³ cells/well) were treated with or without IFNγ for 48 hours. Proliferation was assessed using a CCK8 Kit (n = 3). Data were analyzed with one-way ANOVA. **B,** A549-shCtrol and A549-shZEB1 cells were seeded in 6-well plates at a density of 800 cells per well and maintained for 14 days with or without IFNγ. The medium was changed every 3 days. A549-shControl and A549-shZEB1 cells were seeded in 6-well plates and cultured for 24 hours. Then the cells were stimulated with or without IFNγ (100 IU/mL) for 48 hours. The mRNA levels of (**C**) Cyclin E and (**D**) STAT1 and IRF1 were quantified by RT-PCR. Data are presented as mean ± SD (n = 3) and were analyzed with one-way ANOVA. **E,** A549-shControl and A549-shZEB1 cells were stimulated with or without IFNγ for 48 hours and harvested. STAT1 and IRF1 protein levels were analyzed by immunoblot. **F,** A549-shControl and A549-shZEB1 cells were stimulated with or without IFNγ for indicated time intervals. STAT1 phosphorylation was analyzed by immunoblot. **G,** A549-shControl and A549-shZEB1 cells were seeded in 6-well plates for 24 hours. Then the cells were stimulated with or without IFNγ (100 IU/mL) for 48 hours. The mRNA levels of CXCL9 and CXCL10 were quantified by RT-PCR. Data are presented as the mean ± SD (n = 3) and were analyzed with one-way ANOVA (***, P < 0.001). **H,** A549-shControl and A549-shZEB1 cells were seeded in 6-well plates for 24 hours. Cell-free supernatants were collected after stimulation with or without IFNγ (100 IU/mL) for 48 hours, and CXCL-10 protein levels were measured by ELISA.

were observed after prolonged exposure to IFNγ. Functionally, IFNγ promoted cell migration and metastasis in vivo. (ii) IFNγ stimulation resulted in upregulation of JMJD3 and hence decreased H3K27 trimethylation in the promoter region of ZEB1, increasing ZEB1 expression. (iii) Increased ZEB1 expression mediated IFNγ-induced EMT. (iv) Knockdown of ZEB1 abrogated IFNγ-induced EMT and PD-L1 expression. (v) Inhibition or downregulation of ZEB1 did not affect IFNγ-mediated antitumor effects, including its suppression of cell proliferation and the increase in CXCL9 and CXCL10 expression, which promotes the recruitment of T cells to the tumor microenvironment. On the based on our findings, we propose that the IFNγ-induced upregulation of ZEB1 might increase the aggressiveness of lung cancer cells. Targeting ZEB1 eliminates the protumor effects of IFNγ while retaining its antitumor functions.

Our results showed that IFNγ stimulation induced a dramatic change in the expression pattern of E-cadherin and Vimentin in lung cancer cells. It is widely recognized that experimental models using only a small selection of epithelial and mesenchymal biomarkers, including E-cadherin, N-cadherin, and Vimentin, to define or confirm EMT sketch an oversimplified view of this complex process. EMT is not one clearly defined tumor state but a set of multiple dynamic transitional states between epithelial and mesenchymal phenotypes (16, 34). Because of the complexity of the EMT process, reliable biomarkers are still lacking and a comprehensive method to identify and/or measure EMT, particularly in vivo, does not exist. Nevertheless, numerous gene expression studies have been conducted to obtain transcriptome signatures and marker genes associated with EMT (20, 35). In our study, we not only analyzed CDH1 and VIM

expression levels, but we also performed a transcriptome analysis to determine whether IFNγ alters the expression of other EMT-associated genes. We obtained the EMT core gene signatures, which consists of 130 genes, through a meta-analysis of 18 independent and published gene expression studies of EMT (21). Comparing the expression levels of these 130 genes, we found that IFNγ stimulation altered the transcription of almost 50% of EMT-associated genes in both A549 and HCC827 cells. Among these differentially expressed genes, the EMT-associated transcription factor ZEB1 was rapidly upregulated in response to IFNγ stimulation. In addition to these genetic biomarkers, several *in vitro* criteria have been used to determine EMT, including a spindle-shape morphology and increased migratory capability (36, 37). We found that exposure of lung cancer cells to IFNγ induced morphologic changes, and also promoted cell migration *in vitro* and metastasis *in vivo*. Our findings demonstrate that IFNγ is capable of inducing EMT in lung adenocarcinoma cells.

In prostate cancer and renal cancer, IFNγ induces EMT through the IFIT5–XRN1 complex, which regulates the turnover of specific tumor-suppressive miRNAs, such as miR-101, miR-128, and miR-363 (13). In our study, IFNγ treatment even upregulated *miR-363* levels in lung cancer cells. Our findings suggest that the mechanism by which IFNγ induced EMT is cancer type-dependent and context-specific. In lung cancer cells, IFNγ stimulation led to a rapid increase in mRNA and protein levels of the STAT1-target gene *JMJD3*. In mammary epithelial cells, JMJD3 mediates TGFβ induced EMT through upregulation of *SNAIL* expression, leading to breast cancer invasion (38). JMJD3 upregulates Slug and promotes cell migration, invasion, and transition towards a stem-like phenotype in hepatocellular carcinoma (39). JMJD3 could be a key regulator of cancer aggressiveness. We found that targeting JMJD3 with the inhibitor GSK-J4 or JMJD3 knockdown using siRNA abrogated IFNγ-induced ZEB1 expression.

Recently obtained evidence has indicated that EMT-associated transcription factors regulate a large set of cancer cell features, extending beyond tumor migration, invasion, and metastasis. Recent studies have demonstrated a robust correlation between EMT score, ZEB1/miR-200 levels, and PD-L1 expression in multiple cancer datasets (31). In this study, we showed that IFNγ-induced ZEB1 expression is involved in the upregulation of PD-L1 expression through its suppressive effects on *miR-200* expression. Moreover, Lou

and colleagues have reported that an EMT-related mRNA signature is associated with increased expression of diverse immune inhibitory ligands and receptors in lung adenocarcinoma, including PD-L1, TIM-3, LAG3, and CTLA-4 (40). As illustrated in our working model, IFNγ can simultaneously induce EMT-like features and PD-L1 expression in lung cancer cells via the upregulation of ZEB1 expression. However, whether these two events are independent remains to be elucidated. Our findings suggest that strong antitumor immune properties might be accompanied by increased tumor progression through multiple means.

In this study, downregulation of ZEB1 did not affect IFNγ-mediated suppression of cell proliferation and increased expression of *CXCL9* and *CXCL10*. JMJD3 inhibitor GSK-J4 suppressed IFNγ-induced ZEB1 expression. GSK-J4 has been applied in the treatment of several cancers, such as acute myeloid leukemia and prostate cancer (41, 42). Our study sheds light on the functional mechanism by which targeting ZEB1 might limit the protumor effects of IFNγ.

Authors' Disclosures

No disclosures were reported.

Authors' Contributions

J. Yang: Data curation, formal analysis, investigation, methodology, writing–original draft, writing–review and editing. **X. Wang:** Data curation, formal analysis, methodology. **B. Huang:** Data curation, formal analysis, methodology, writing–review and editing. **R. Liu:** Methodology. **H. Xiong:** Methodology, writing–review and editing. **F. Ye:** Methodology. **C. Zeng:** Methodology. **X. Fu:** Conceptualization, investigation, writing–review and editing. **L. Li:** Conceptualization, resources, formal analysis, supervision, funding acquisition, validation, methodology, writing–original draft, writing–review and editing.

Acknowledgments

References

1. Ivashkiv LB. IFNγ: signalling, epigenetics and roles in immunity, metabolism, disease and cancer immunotherapy. Nat Rev Immunol 2018;18: 545–58.
2. Gao Y, Yang J, Cai Y, Fu S, Zhang N, Fu X, et al. IFN-γ-mediated inhibition of lung cancer correlates with PD-L1 expression and is regulated by PI3K-AKT signaling. Int J Cancer 2018;143:931–43.
3. Garris CS, Arlauckas SP, Kohler RH, Trefny MP, Garren S, Piot C, et al. Successful Anti-PD-1 cancer immunotherapy requires T cell-dendritic cell crosstalk involving the cytokines IFN-γ and IL-12. Immunity 2018;49:1148–61 e7.
4. Gao J, Shi LZ, Zhao H, Chen J, Xiong L, He Q, et al. Loss of IFN-γ pathway genes in tumor cells as a mechanism of resistance to Anti-CTLA-4 therapy. Cell 2016; 167:397–404 e9.
5. Zaretsky JM, Garcia-Diaz A, Shin DS, Escuin-Ordinas H, Hugo W, Hu-Lieskovan S, et al. Mutations associated with acquired resistance to PD-1 blockade in melanoma. N Engl J Med 2016;375:819–29.
6. Shin DS, Zaretsky JM, Escuin-Ordinas H, Garcia-Diaz A, Hu-Lieskovan S, Kalbasi A, et al. Primary resistance to PD-1 blockade mediated by JAK1/2 mutations. Cancer Discov 2017;7:188–201.
7. Chow MT, Ozga AJ, Servis RL, Frederick DT, Lo JA, Fisher DE, et al. Intratumoral activity of the CXCR3 chemokine system is required for the efficacy of anti-PD-1 therapy. Immunity 2019;50:1498–512 e5.
8. Han X, Wang Y, Sun J, Tan T, Cai X, Lin P, et al. Role of CXCR3 signaling in response to anti-PD-1 therapy. EBioMedicine 2019;48:169–77.
9. Mandai M, Hamanishi J, Abiko K, Matsumura N, Baba T, Konishi I. Dual faces of IFNγ in cancer progression: a role of PD-L1 induction in the determination of pro- and antitumor immunity. Clin Cancer Res 2016;22: 2329–34.
10. Minn AJ, Wherry EJ. Combination cancer therapies with immune checkpoint blockade: convergence on interferon signaling. Cell 2016; 165:272–5.
11. Bellucci R, Martin A, Bommarito D, Wang K, Hansen SH, Freeman GJ, et al. Interferon-γ-induced activation of JAK1 and JAK2 suppresses tumor cell susceptibility to NK cells through upregulation of PD-L1 expression. Oncoimmunology 2015;4:e1008824.
12. Benci JL, Xu B, Qiu Y, Wu TJ, Dada H, Twyman-Saint Victor C, et al. Tumor interferon signaling regulates a multigenic resistance program to immune checkpoint blockade. Cell 2016;167:1540–54 e12.

13. Lo UG, Pong RC, Yang D, Gandee L, Hernandez E, Dang A, et al. IFNγ-Induced IFIT5 promotes epithelial-to-mesenchymal transition in prostate cancer via miRNA processing. Cancer Res 2019;79:1098–112.

14. Chaffer CL, San Juan BP, Lim E, Weinberg RA. EMT, cell plasticity and metastasis. Cancer Metastasis Rev 2016;35:645–54.

15. Goossens S, Vandamme N, Van Vlierberghe P, Berx G. EMT transcription factors in cancer development re-evaluated: beyond EMT and MET. Biochim Biophys Acta Rev Cancer 2017;1868:584–91.

16. Nieto MA, Huang RY, Jackson RA, Thiery JP. Emt: 2016. Cell 2016;166:21–45.

17. De Craene B, Berx G. Regulatory networks defining EMT during cancer initiation and progression. Nat Rev Cancer 2013;13:97–110.

18. Karagiannis GS, Pastoriza JM, Wang Y, Harney AS, Entenberg D, Pignatelli J, et al. Neoadjuvant chemotherapy induces breast cancer metastasis through a TMEM-mediated mechanism. Sci Transl Med 2017;9.

19. Ravindranathan P, Lee TK, Yang L, Centenera MM, Butler L, Tilley WD, et al. Peptidomimetic targeting of critical androgen receptor-coregulator interactions in prostate cancer. Nat Commun 2013;4:1923.

20. Byers LA, Diao L, Wang J, Saintigny P, Girard L, Peyton M, et al. An epithelial-mesenchymal transition gene signature predicts resistance to EGFR and PI3K inhibitors and identifies Axl as a therapeutic target for overcoming EGFR inhibitor resistance. Clin Cancer Res 2013;19:279–90.

21. Groger CJ, Grubinger M, Waldhor T, Vierlinger K, Mikulits W. Meta-analysis of gene expression signatures defining the epithelial to mesenchymal transition during cancer progression. PLoS One 2012;7:e51136.

22. Zhu X, Zhong J, Zhao Z, Sheng J, Wang J, Liu J, et al. Epithelial derived CTGF promotes breast tumor progression via inducing EMT and collagen I fibers deposition. Oncotarget 2015;6:25320–38.

23. Wang K, Ji W, Yu Y, Li Z, Niu X, Xia W, et al. FGFR1-ERK1/2-SOX2 axis promotes cell proliferation, epithelial-mesenchymal transition, and metastasis in FGFR1-amplified lung cancer. Oncogene 2018;37:5340–54.

24. Roof DJ, Hayes A, Adamian M, Chishti AH, Li T. Molecular characterization of abLIM, a novel actin-binding and double zinc finger protein. J Cell Biol 1997;138:575–88.

25. Chaffer CL, Marjanovic ND, Lee T, Bell G, Kleer CG, Reinhardt F, et al. Poised chromatin at the ZEB1 promoter enables breast cancer cell plasticity and enhances tumorigenicity. Cell 2013;154:61–74.

26. Gao Y, Zhao Y, Zhang J, Lu Y, Liu X, Geng P, et al. The dual function of PRMT1 in modulating epithelial-mesenchymal transition and cellular senescence in breast cancer cells through regulation of ZEB1. Sci Rep 2016;6:19874.

27. Przanowski P, Dabrowski M, Ellert-Miklaszewska A, Kloss M, Mieczkowski J, Kaza B, et al. The signal transducers Stat1 and Stat3 and their novel target Jmjd3 drive the expression of inflammatory genes in microglia. J Mol Med (Berl) 2014; 92:239–54.

28. Heinemann B, Nielsen JM, Hudlebusch HR, Lees MJ, Larsen DV, Boesen T, et al. Inhibition of demethylases by GSK-J1/J4. Nature 2014;514:E1–2.

29. Guenther MG, Levine SS, Boyer LA, Jaenisch R, Young RA. A chromatin landmark and transcription initiation at most promoters in human cells. Cell 2007;130:77–88.

30. Burk U, Schubert J, Wellner U, Schmalhofer O, Vincan E, Spaderna S, et al. A reciprocal repression between ZEB1 and members of the miR-200 family promotes EMT and invasion in cancer cells. EMBO Rep 2008;9:582–9.

31. Chen L, Gibbons DL, Goswami S, Cortez MA, Ahn YH, Byers LA, et al. Metastasis is regulated via microRNA-200/ZEB1 axis control of tumour cell PD-L1 expression and intratumoral immunosuppression. Nat Commun 2014;5:5241.

32. Yano T, Sugio K, Yamazaki K, Kase S, Yamaguchi M, Ondo K, et al. Direct IFNluence of interferon-γ on proliferation and cell-surface antigen expression of non-small cell lung cancer cells. Lung Cancer 2000;30:169–74.

33. Ohtsubo M, Theodoras AM, Schumacher J, Roberts JM, Pagano M. Human cyclin E, a nuclear protein essential for the G1-to-S phase transition. Mol Cell Biol 1995;15:2612–24.

34. Pastushenko I, Blanpain C. EMT transition states during tumor progression and metastasis. Trends Cell Biol 2019;29:212–26.

35. Tan TZ, Miow QH, Miki Y, Noda T, Mori S, Huang RY, et al. Epithelial-mesenchymal transition spectrum quantification and its efficacy in deciphering survival and drug responses of cancer patients. EMBO Mol Med 2014;6:1279–93.

36. Zeisberg M, Neilson EG. Biomarkers for epithelial-mesenchymal transitions. J Clin Invest 2009;119:1429–37.

37. Krebs AM, Mitschke J, Lasierra Losada M, Schmalhofer O, Boerries M, Busch H, et al. The EMT-activator Zeb1 is a key factor for cell plasticity and promotes metastasis in pancreatic cancer. Nat Cell Biol 2017;19:518–29.

38. Ramadoss S, Chen X, Wang CY. Histone demethylase KDM6B promotes epithelial-mesenchymal transition. J Biol Chem 2012;287:44508–17.

39. Tang B, Qi G, Tang F, Yuan S, Wang Z, Liang X, et al. Aberrant JMJD3 expression upregulates slug to promote migration, invasion, and stem cell-like behaviors in hepatocellular carcinoma. Cancer Res 2016;76:6520–32.

40. Lou Y, Diao L, Cuentas ER, Denning WL, Chen L, Fan YH, et al. Epithelial-mesenchymal transition is associated with a distinct tumor microenvironment including elevation of inflammatory signals and multiple immune checkpoints in lung adenocarcinoma. Clin Cancer Res 2016;22:3630–42.

41. Li Y, Zhang M, Sheng M, Zhang P, Chen Z, Xing W, et al. Therapeutic potential of GSK-J4, a histone demethylase KDM6B/JMJD3 inhibitor, for acute myeloid leukemia. J Cancer Res Clin Oncol 2018;144:1065–77.

42. Morozov VM, Li Y, Clowers MM, Ishov AM. Inhibitor of H3K27 demethylase JMJD3/UTX GSK-J4 is a potential therapeutic option for castration resistant prostate cancer. Oncotarget 2017;8:62131–42.

Molecular Cancer Research

An IFNγ/STAT1/JMJD3 Axis Induces ZEB1 Expression and Promotes Aggressiveness in Lung Adenocarcinoma

Jianjian Yang, Xue Wang, Bing Huang, et al.

Updated version	Access the most recent version of this article at: doi:10.1158/1541-7786.MCR-20-0948
Supplementary Material	Access the most recent supplemental material at: http://mcr.aacrjournals.org/content/suppl/2021/03/24/1541-7786.MCR-20-0948.DC1

Cited articles	This article cites 41 articles, 11 of which you can access for free at: http://mcr.aacrjournals.org/content/19/7/1234.full#ref-list-1

E-mail alerts	Sign up to receive free email-alerts related to this article or journal.
Reprints and Subscriptions	To order reprints of this article or to subscribe to the journal, contact the AACR Publications Department at pubs@aacr.org.
Permissions	To request permission to re-use all or part of this article, use this link http://mcr.aacrjournals.org/content/19/7/1234. Click on "Request Permissions" which will take you to the Copyright Clearance Center's (CCC) Rightslink site.